PROCEEDINGS OF SPIE

SPIEDigitalLibrary.org/conference-proceedings-of-spie

Low-voltage capacitive measurement methodology for dielectric elastomers

Peranich, Preston, Carroll, Will, Middleton, Carver, Parker, Erin, Prabhakar, Samuel, et al.

Preston Peranich, Will Carroll, Carver Middleton, Erin Parker, Samuel Prabhakar, Purva Talegaonkar, Samaneh Davarzani, David Saucier, Karen Persons, John E. Ball, Reuben Burch, Harish Chander, Adam Knight, Brian Smith, "Low-voltage capacitive measurement methodology for dielectric elastomers," Proc. SPIE 11757, Smart Biomedical and Physiological Sensor Technology XVIII, 1175707 (12 April 2021); doi: 10.1117/12.2587797



Event: SPIE Defense + Commercial Sensing, 2021, Online Only

Low-voltage capacitive measurement methodology for dielectric elastomers

Preston Peranich^a, Will Carroll^a, Carver Middleton^a, Erin Parker^a, Samuel Prabhakar^a, Purva Talegaonkar^a, Samaneh Davarzani^a, David Saucier^a, Karen Persons^a, John E. Ball^a, Reuben Burch^a, Harish Chander^a, Adam Knight^a, and Brian Smith^a

^aMississippi State University, Starkville, Mississippi, USA

ABSTRACT

Dielectric elastomers have emerged in recent years as a smart material capable of acting as an actuator, a sensor, or a generator. When used as a sensor, this soft, flexible material exhibits a change in capacitance as it is deformed in both compression and tension. This has led to the adaptation of dielectric elastomer sensors in the wearable technology space, where careful sensor placement can enable the measurement of biomechanical movement. However, these sensors may not be measured using traditional capacitance measurement techniques due to their increased electrode resistance. Thus, a low frequency, low voltage capacitive measurement methodology needs to be derived for these sensors to thrive in wearable applications. In this work, we propose such a methodology which utilizes phase detection with the Goertzel algorithm. Traditionally used for tone detection, the Goertzel algorithm provides an efficient method for recovering individual terms of the DFT. Our sensing methodology is integrated into a low-cost microcontroller and integrated with a wireless microcontroller to enable remote measurement of the dielectric elastomers. The open sourcing of this device may jump-start the widespread adoption of dielectric elastomers as biomechanical sensors.

Keywords: Electroactive polymer, stretch sensor, soft robotic sensor, goertzel, dielectric elastomer

1. INTRODUCTION

Biomechanical measurement and analyses of human movement has evolved over time from using simple goniometric devices to the full-fledged motion capture systems of today. With this increase in technological capabilities, a wide array of fields have found tremendous value in the data products produced by state of the art equipment. Clinical research uses such information to analyze gait characteristics and diagnose disease. Strength and conditioning coaches have used motion capture systems and accelerometer devices to analyze athlete performance and identify areas for improvement. However, current motion capture systems are typically composed of a large array of cameras that must be calibrated and are mounted in semi-permanent positions. Additionally, motion capture systems incur a large financial and time cost to use. In recent years, wearable technology solutions have been created with the aim to accomplish a similar result as the motion capture system, while packaged in a wearable device. Many of these attempts utilize a combination of accelerometers and inertial measurement units (IMU). However, research has come to light indicating that IMUs may be subject to significant drift, leading to an inaccurate data product. Thus, there is still a need for a wearable technology system that is capable of generating data products with the same quality as from motion capture system, but with greater portability and reduced cost.

Recently, a class of material known as electroactive polymers (EAP) have been growing popularity due to their muscle-like ability to change shape when stimulated with an electric field. Exploiting this property allows the material to act as either an actuactor, when an electrical signal is converted to mechanical deformation, or sensor, when a mechanical deformation is converted to electrical energy. A subclass of EAPs, known as dielectric elastomers (DE), have been subject to a large amount of research in the robotics space since they can be used as a type of artificial muscle. DEs are constructed by coating a thin electrode material on either side of a thin elastic dielectric film and are usually much more flexible than traditional EAPs. In essence, DEs electrically resemble a deformable capacitor, where the stretching or compression of the material results in a change in capacitance. Naturally, DEs are better suited to adoption in the wearable technology space since the sensors

Smart Biomedical and Physiological Sensor Technology XVIII, edited by Brian M. Cullum, Douglas Kiehl, Eric S. McLamore, Proc. of SPIE Vol. 11757, 1175707 · © 2021 SPIE CCC code: 0277-786X/21/\$21 · doi: 10.1117/12.2587797



Figure 1. Sock Prototype.

are much more conformable to irregular surfaces than traditional strain gauges. This means these sensors can be integrated into clothing an stretched without significant interference to the user. The work presented in Ref. 11 has evaluated the use of this type of sensor material, specifically using StretchSense^{TM} sensors, in a wearable sock to capture foot-ankle kinematics in real-time with positive results. Fig. 1 shows the current sock prototype which features integrated DE sensors and on-board sensing circuitry with Bluetooth radio. Unfortunately, measuring the capacitance of a DE is more complex than that of a typical discrete capacitor, and a need has developed for a low-cost low-voltage capacitive sensing solution that can be integrated into a small wearable device.

2. BACKGROUND

As described in Sec. 1, the basic structure of a DE resembles that of a capacitor: two conductive electrodes with a dielectric between. Hence, the capacitance of the sensor is dependent on the physical properties, just as in a traditional capacitor:

$$C = \frac{\epsilon_r \epsilon_0 A}{d} \tag{1}$$

Where ϵ_r is the relative permittivity of the dielectric material, ϵ_0 is the permittivity of free space, A is the area of the electrodes, and d is the distance separating the electrodes. However, in a DE, both the area of the electrodes and the distance between the electrodes changes as the elastomer is deformed. This means both stretch along the sensor and compression normal to the sensor will result in a change in capacitance. The relation between stretch and change in capacitance is linear.

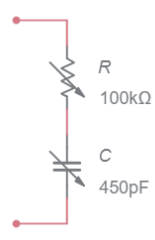


Figure 2. Basic electrical model of a dielectric elastomer.

The basic electrical model of the dielectric elastomer, shown in Fig. 2, also mirrors that of a traditional capacitor, with a resistor in series with the capacitor to represent the electrode resistance. Unlike a traditional capacitor, both the electrode resistance and capacitance of the sensor can vary widely depending on the stretch induced to the sensor. On top of this, the electrode resistance of a DE sensor is also very large, ¹² so traditional capacitance measurement techniques are unable to accurately measure the capacitance. Though some stretch information may be obtained by measuring the resistance of the sensor, this is prone to error due to the high dependence on temperature for the sensor resistance.

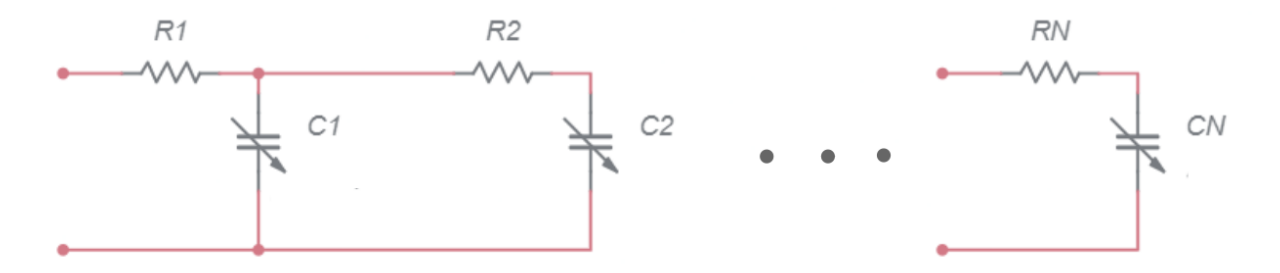


Figure 3. Distributed nature of electrical characteristics in DEs.

Since the electrodes of a DE run along the entire length of a sensor, both the electrode resistance and capacitance is distributed along the length of the sensor, leading to the more advanced electrical model of a DE shown in Fig. 3. Because the capacitance is distributed along the length, a higher frequency signal will not propagate as far along a DE sensor as a low frequency signal. This occurs since the capacitive reactance decreases as the sensing frequency is increased, and, hence, the charge follows the path of least resistance and does not propagate along the entire sensor. Ref. 13 used this attribute advantageously to create a multi-frequency sensing algorithm that could localize the pressure applied to a DE sensor.

3. METHODOLOGY

Motivated by the work in Ref. 14, a capacitive sensing solution was designed. The proposed method utilizes a sinusoidal input signal across an RC circuit configuration, where the DE serves as the capacitor. When presented with a sinusoidal signal, the RC circuit will both attenuate the signal and introduce a phase shift across the capacitor. By measuring the phase shift induced by the RC circuit, the capacitance may be recovered and correlated with the physical deformation of the sensor. To illustrate the change in phase shift at different capacitances, Fig. 7 displays the input voltage signal and sensor voltage signal at two different sensor capacitances, 450pF and 950pF, which fall within the normal operating range of the specific sensor used in this work.

3.1 Capacitance from phase shift

Recovering the capacitance from the phase shift of the voltage across the sensor is quite simple; the voltage at the sensor is related to the input sinusoid following:

$$V_s = V_{in} \frac{X_s}{\sqrt{R^2 + X_s^2}} \tag{2}$$

Where R is the resistor in the RC circuit and X_s is the reactance of the sensor. This sensing circuit will act as a low pass filter with a cutoff frequency and phase shift found using:

$$f_c = \frac{1}{2\pi RC} \tag{3}$$

$$\phi = -\arctan 2\pi fRC \tag{4}$$

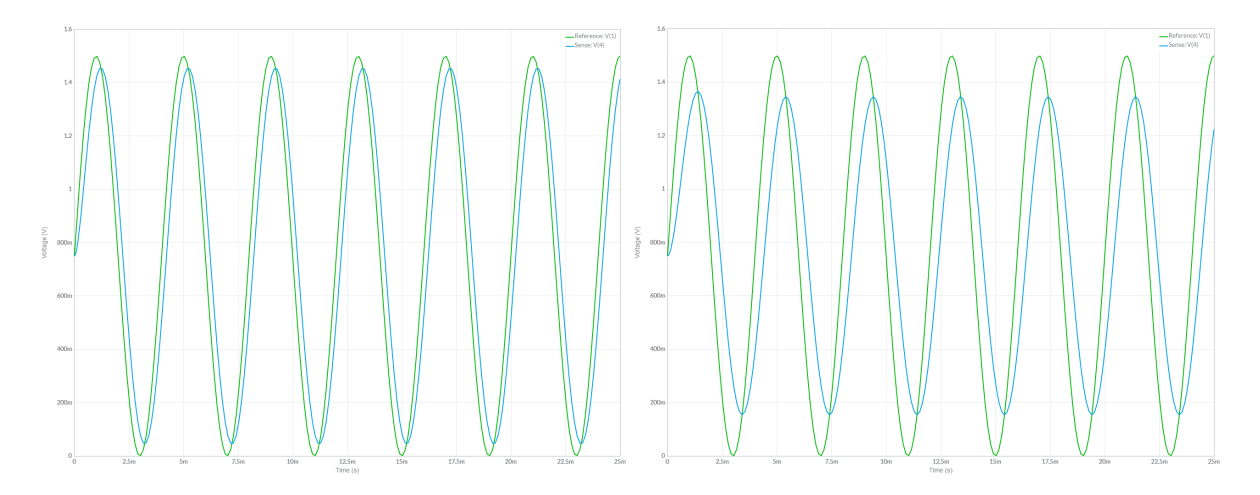


Figure 4. Reference signal vs sensor signal at 450pF (left) and 950pF (right).

Eq. 4 can then be solved for capacitance:

$$C = \frac{\tan -\phi}{2\pi f R} \tag{5}$$

Thus, the capacitance of the DE may be recovered if accurate measurement of the phase shift can be made. As was mentioned in Sec. 2, special attention needs to be paid to the selection of the sensing frequency in this application. Following the simulation results in Ref. 13, a sensing frequency of 250Hz was selected for this design. This frequency is sufficiently low as to allow propagation of the signal along the entire sensor length. A $510k\Omega$ resistor was selected for this design, which will have the added benefit of filtering unwanted noise from the signal prior to sampling. The input sinusoid has an amplitude of 0.75V and is offset such that the voltage will oscillate between 0 and 1.5V. It will be generated from a Digital to Analog (DAC) converter using a look up table (LUT) which updates the output to generate the sinusoid at the specified frequency. The sensing circuit schematic is shown in Fig. 5. It is important to note that the same input signal may be fed to any number of RC circuits for measurement of phase, as long as there are enough Analog to Digital (ADC) channels to sample the sensor signal. Lastly, a unity gain buffer was added to buffer the voltage across the sensor for the ADC converter so that the ADC converter does not affect the sensor signal. The unity gain buffer has high input impedance so it will negligibly affect the sensing circuit.

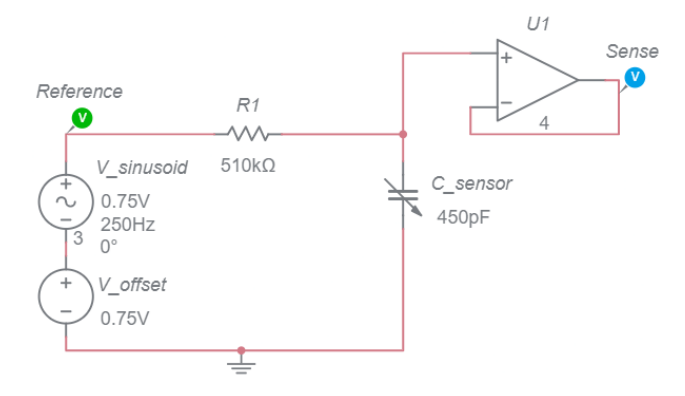


Figure 5. Capacitive sensing circuit.

3.2 Phase Measurement

The most essential operation of the candidate sensing solution is correct measurement of sensor signal phase. When posed with the problem of measuring phase, many engineers will utilize the tried and tested Fast Fourier Transform (FFT) as the algorithm of choice for extracting frequency information from a signal. However, the FFT is a computationally expensive algorithm and is quite inefficient on low-cost low-power embedded hardware. Additionally, the FFT calculates frequency content for many different bins, but in this application, we know exactly which frequency to measure. The Goertzel algorithm¹⁵ circumvents this problem and has proven to be an efficient method for the evaluation of single terms of a DFT. If computing just a single term of a DFT, the Goertzel algorithm has a computational complexity of just O(N) whereas the FFT has a complexity of $O(N \log N)$ where N is the number of samples in each calculation. Historically, this algorithm has been used for tone detection of a keypad on an analog phone, but by adapting this algorithm for this application, phase information may be calculated in real-time on low-cost embedded hardware. Additionally, the Goertzel algorithm utilizes real-valued arithmetic in it's computation, making implementation on embedded architectures even easier.

The Goertzel algorithm, similar to the FFT, uses a block size to control the frequency resolution. The block size should be selected such that the sampling frequency $f_{sampling}$ divided by the block size N is an integer multiple of the target frequency f_{target} :

$$\frac{f_{sampling}}{N} = f_{target} * a, a = 1, 2, 3, \dots$$
 (6)

To compute the Goertzel algorithm, the following coefficients should be calculated before runtime once your sampling rate, target frequency, and block size are identified:

$$k = int(0.5 + \frac{Nf_{target}}{f_{sampling}}) \tag{7}$$

$$w = \frac{2\pi k}{N} \tag{8}$$

$$c = \cos w \tag{9}$$

$$s = \sin w \tag{10}$$

$$a = 2c \tag{11}$$

Now, the Goertzel may be calculated as shown in Fig. 6. In this implementation, we are only considered about phase information and not magnitude.

Figure 6. Psuedo code for the Goertzel algorithm. Repeated for each block of samples.

For this work, the Goertzel algorithm was first implemented in Python. Here, it was tested alongside a traditional DFT and a phase LUT to ensure the correct phase information was recovered from the signal.

A synthetic 250Hz sinusoidal signal was synthesized at a sampling frequency of 2kHz, with a corresponding LUT to match the phase of a sinusoid through it's period. The synthesized samples were added to buffers and the corresponding DFT and Goertzel algorithms were calculated once a sufficient number of samples had accumulated. Fig. 7 shows the calculated phase of the three methods, all of which produced the same result. This verifies the correct operation of the Goertzel implementation, so a more thorough implementation of the capacitive sensing solution may now be carried out.

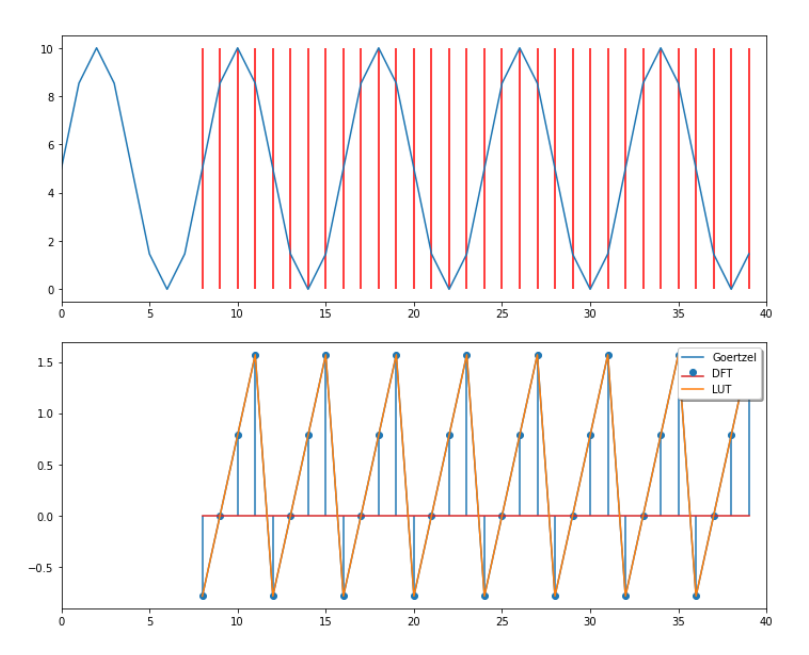


Figure 7. Comparison between Goertzel, DFT, and ground-truth phase LUT. The top plot shows the synthesized signal (blue) and vertical markers where DFT and Goertzel calculations were triggered (red). The bottom plot compares the results of the DFT and Goertzel with the ground-truth phase information.

4. IMPLEMENTATION

With the underlying methodology established for the capacitive sensing solution, a two-step approach was taken to bring this solution to fruition. First, a simulation was created using Python to prototype algorithms and verify the methodology could be implemented in an ideal scenario. Following a successful simulation, the algorithms would be ported to the target embedded device and all accompanied configuration would be added.

4.1 Simulation Results

As mentioned above, Python was used to simulate the algorithms and sensor signals to validate the methodology. To begin, a floating point approach was taken, which would allow for fast prototyping of the algorithm without the need to monitor the values of each portion of the Goertzel algorithm for overflows. The sampling rate was set to 2kHz based on hardware capabilities and the corresponding block size was calculated in accordance with Eq. 6. After these parameters were set, the reference and sensor signals were created using the phase offset and impedance calculated for the chosen resistor and base capacitance. The synthesized signals, shown in Fig. 8, range from 0 to 4095 to match the dynamic range of the embedded hardware 12-bit ADC. Since the embedded hardware will be responsible for creating the sinusoid, it will have real-time information of the phase of the input sinusoid. Therefore, we will not need to sample and calculate the phase for the reference signal in this implementation. Now, the Goertzel algorithm implemented in Sec. 3 may be used on the synthesized sensor samples, with the measured phase then compared to the current output phase to establish the relative phase between the two signals. Afterwards, the capacitance can be recovered and the methodology may be evaluated.

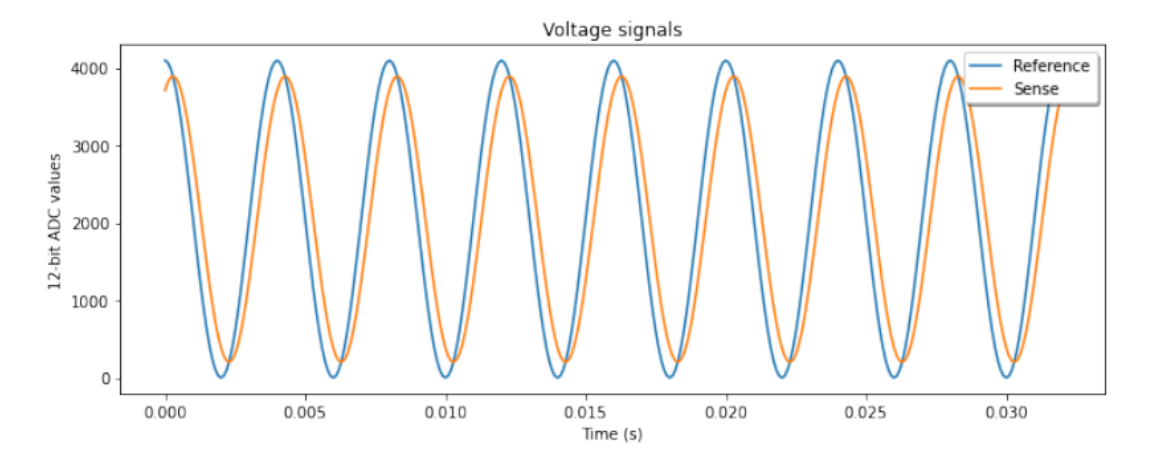


Figure 8. Simulated reference and sensor signals.

After positive results were achieved using a constant capacitance, a time-varying capacitance signal was generated for the purpose of evaluating how the algorithm would perform while the sensor is stretched. A triangular wave capacitance signal was designed, with the corresponding voltage signals synthesized. Fig. 9 shows that the recovered capacitance tracks the true capacitance very well, once again verifying the algorithm fundamentals.

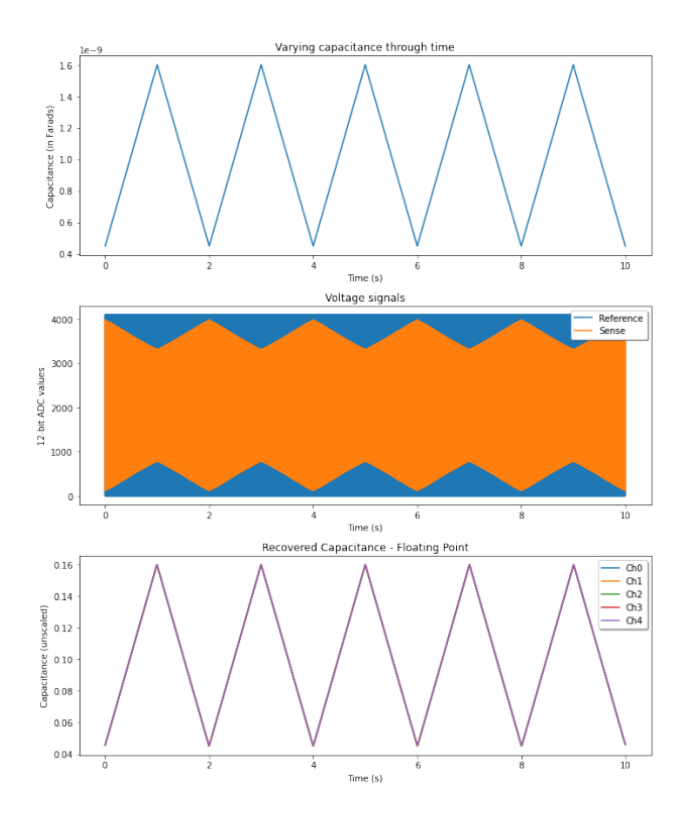


Figure 9. Simulated time varying capacitance with recovered capacitance with floating-fixed-point.

At this stage, a fixed-point processing approach was developed in simulation as well. This further eases the difficulty of implementation at the embedded level, since it offers the advantage of optimizing the fixed-point

arithmetic in Python instead of C or C++. A Python package for fixed-point math was found and used to build out a library of functions which directly mirror those available on the candidate embedded device. This library notified the user of overflows when running the algorithms, so the precision at each step of the algorithm could be optimized to utilize the largest amount of dynamic range without worry of errors when ran on the hardware. A capacitance range larger than that found on the real sensors was swept to ensure no precision issues were present in the fixed-point process. The fixed-point results were then compared to the floating point results, shown in Fig. 10. Impressively, the fixed-point recovered capacitance was only 2pF off the true capacitance over the simulation, which stepped capacitance from 450pF to 1650pF. Porting this optimized fixed-point Python code to the embedded hardware will be a light task since the library functions used mirror that of the embedded fixed-point library.

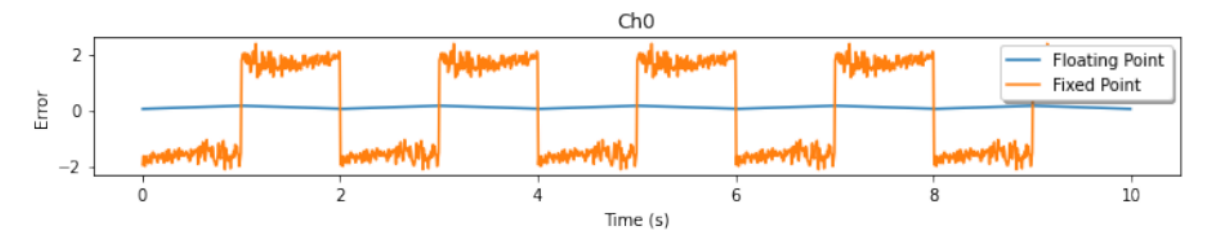


Figure 10. Error (in pF) between the actual capacitance and recovered capacitance for floating- and fixed-point algorithms.

4.2 Embedded Progress

An initial implementation effort has commenced using a Ti MSP430 family microcontroller. This platform allows for low power consumption and should provide enough computational power for the needs of this solution. Following the verification of the working algorithm in the simulation, it has been ported to the embedded device. Dummy data has been input into the embedded Goertzel implementation and the results have been verified to match that of the simulation. Additionally, the embedded implementation communicates with a separate board, using SPI, to relay information over a Bluetooth connection to a host computer which records the sensor data. The SPI communication link has been verified working as well, with the ability to send configuration messages to the device to set number of sensor channels, output data rate, and more. A lookup table (LUT) is created and afterward used by the onboard DAC to generate the input sinusoid at a frequency of 250 Hz. The DAC output has been verified and shown to be quite stable over even large time frames. The ADC peripheral of the module has been configured to routinely sample a channel and switch to the next channel. It has been verified to work with steady DC signals, but some investigation still needs to be performed to determine if the ADC sample and hold time is long enough to charge the internal capacitor closer to the actual sensor voltage.

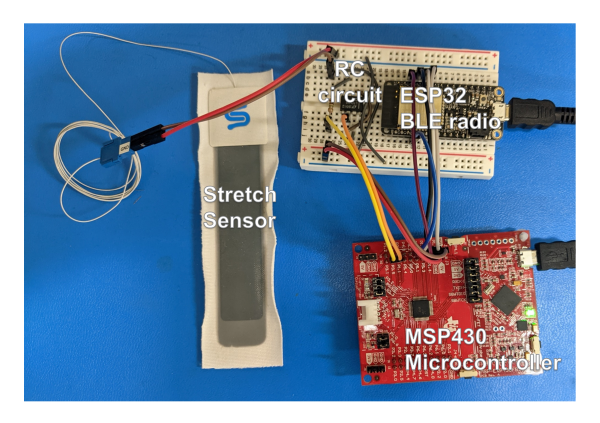


Figure 11. Embedded hardware layout.

The implementation of each of the above systems has required careful consideration of program flow and code optimization to reduce interrupt lengths. Even with such optimizations, the current status of the implementation

appears to be utilizing the microcontroller at or above computational capacity. Further investigation may motivate a switch to the MSP432 family of devices, which may run an Real-time Operating System (RTOS) to better guarantee that timing requirments for this application are met.

5. CONCLUSION

The current work offers a unique approach to the measurement of DEs with a low-voltage sensing signal. Such an approach, implemented on a small PCB, could see the adaption of DEs in a larger number of applications due to the unique properties of DEs. Once the embedded design has been debugged and verified against current methods, the goal is to open-source the developed software so the larger scientific community can use and adapt this implementation to accelerate adoption of DEs. The simulation code used for this project has been open-sourced now and may be accessed at https://github.com/msstate-athlete-engineering/soft-sensors-research. In the case of wearable technology, efficient and accurate measurement of DEs will better improve final data products and lead to more confidence in the function of the wearable platform.

ACKNOWLEDGMENTS

We would like to acknowledge the funding provided to the Mississippi State Athlete Engineering Group by the National Science Foundation, without which this research may not have been able to be carried out.

REFERENCES

- [1] Son, S. J., Kim, H., Seeley, M. K., and Hopkins, J. T., "Altered walking neuromechanics in patients with chronic ankle instability," *Journal of athletic training* **54**(6), 684–697 (2019).
- [2] Staranowicz, A., Brown, G. R., and Mariottini, G.-L., "Evaluating the accuracy of a mobile kinect-based gait-monitoring system for fall prediction," in [Proceedings of the 6th international conference on PErvasive technologies related to assistive environments], 1–4 (2013).
- [3] Luczak, T., Saucier, D., Burch V, R. F., Ball, J. E., Chander, H., Knight, A., Wei, P., Iftekhar, T., et al., "Closing the wearable gap: Mobile systems for kinematic signal monitoring of the foot and ankle," *Electronics* 7(7), 117 (2018).
- [4] Namal, S., Senanayake, A., Chong, V., Chong, J., and Sirisinghe, G. R., "Analysis of soccer actions using wireless accelerometers," in [2006 4th IEEE International Conference on Industrial Informatics], 664–669, IEEE (2006).
- [5] Davarzani, S., Saucier, D., Peranich, P., Carroll, W., Turner, A., Parker, E., Middleton, C., Nguyen, P., Robertson, P., Smith, B., et al., "Closing the wearable gap—part vi: Human gait recognition using deep learning methodologies," *Electronics* 9(5), 796 (2020).
- [6] Filippeschi, A., Schmitz, N., Miezal, M., Bleser, G., Ruffaldi, E., and Stricker, D., "Survey of motion tracking methods based on inertial sensors: A focus on upper limb human motion," Sensors 17(6), 1257 (2017).
- [7] Bar-Cohen, Y., "Electroactive polymers: current capabilities and challenges," in [Smart Structures and Materials 2002: Electroactive Polymer Actuators and Devices (EAPAD)], 4695, 1–7, International Society for Optics and Photonics (2002).
- [8] Bar-Cohen, Y., "Electroactive polymers as artificial muscles: A review," Journal of Spacecraft and Rockets 39(6), 822–827 (2002).
- [9] Keplinger, C., Kaltenbrunner, M., Arnold, N., and Bauer, S., "Capacitive extensometry for transient strain analysis of dielectric elastomer actuators," *Applied Physics Letters* **92**(19), 192903 (2008).
- [10] Suo, Z., Zhao, X., and Greene, W. H., "A nonlinear field theory of deformable dielectrics," Journal of the Mechanics and Physics of Solids 56(2), 467–486 (2008).
- [11] Saucier, D., Luczak, T., Nguyen, P., Davarzani, S., Peranich, P., Ball, J. E., Burch, R. F., Smith, B. K., Chander, H., Knight, A., et al., "Closing the wearable gap—part ii: Sensor orientation and placement for foot and ankle joint kinematic measurements," Sensors 19(16), 3509 (2019).

- [12] Carpi, F., Chiarelli, P., Mazzoldi, A., and De Rossi, D., "Electromechanical characterisation of dielectric elastomer planar actuators: comparative evaluation of different electrode materials and different counterloads," Sensors and Actuators A: Physical 107(1), 85–95 (2003).
- [13] Xu, D., Tairych, A., and Anderson, I. A., "Where the rubber meets the hand: Unlocking the sensing potential of dielectric elastomers," *Journal of Polymer Science Part B: Polymer Physics* **54**(4), 465–472 (2016).
- [14] Xu, D., McKay, T. G., Michel, S., and Anderson, I. A., "Enabling large scale capacitive sensing for dielectric elastomers," in [Electroactive Polymer Actuators and Devices (EAPAD) 2014], 9056, 90561A, International Society for Optics and Photonics (2014).
- [15] Goertzel, G., "An algorithm for the evaluation of finite trigonometric series," *The American Mathematical Monthly* **65**(1), 34–35 (1958).